Numerical Simulation of Sintering in the Ceramic Oxide

Dr. (Eng) Mohammed J. Kadhim
University of Technology

Dr.(Eng) Adill A. ALwan
University of Babylon

Dr. (Eng) Elham Abdul M. Ibraheem
Technical Institute of Babylon

Abstract

Sintering process analyzed mathematically by prediction unsteady-state mathematical model in order to give more description and understanding for the mechanism of this process, which includes mass transport that may occur via diffusion.

The spatial and temporal temperature profile with the solid medium has been determined by solving the unsteady state Fourier heat energy transport equation using the explicit finite difference numerical method, which would minimize the solution errors, this leads to more realistic determination of temperature distribution within the work-piece. Alumina has been selected as target to represent nonmetallic material of diverse physical and thermal properties. The average grain size for alumina is 0.5 μm with initial compact density 2160 kg/m^3. These values gave a reliable approach to calculate the porosity and relative strength.

د. محمد جاسم كاظم
الجامعة التكنلوجية

د.عادل عباس علوان
جامعة بابل

د. الهام عبد المجيد ابراهيم
المعهد التقني/ بابل

الخلاصة

عملية التلبيد حللت رياضيا باستخدام معادلات الحالة الغير مستقرة لغرض الحصول على تفسير لفهم ميكانيكية هذه العملية والتي تتضمن انتقال الكتلة خلال عملية الانتشار.

تم احتساب التوزيع الحراري الفضائي داخل الوسط وذلك بحل معادلة (فورير) للتوصيل الحراري باستعمال طريقة الحل العددي البائن للفرو قات الحدية والتي تؤمن أدنى نسبة للخطأ حيث تم تطوير النموذج الرياضي لانتقال الطاقة ليشمل التأثير الحراري على سطح العينة من كل الجوانب وداخل العينة. إن هذا النموذج أعطى قابلية جيدة لحساب الانحدار الحراري العالي في

درجات الحرارة وكذلك حالة عدم الاتزان الحراري و هذا يقود إلى حسابات أكثر واقعية للتوزيع الحراري للوسط وتم فعلا حساب التوزيع الحراري لمادة الألومينا تسخينها في فرن حراري بطاقة حرارية معلومة. وكانت القيمة الأولية للحجم الحبيبي للمادة ٠,٥ μm عند قيم أولية للكثافة ٢١٦٠ kg/m^3 ، وتم أختيار الطريقة المناسبة لحساب المسامية والمقاومة بالاعتماد على هذه القيم.

1. Introduction

Powder technology (P/T) processing has become an advanced important technique, which many materials were produced by these processes by using uniaxial die pressing and sintering. The most important reason to use (P/T) that may materials are difficult to melt and cast, as for example ceramic materials, hard metals, cermets or refractory metals. Another reason for using powder technology may be that it is economically attractive to make mass production complex shaped structural parts by powder compaction and sintering [1].

Sintering is an important technological step in any powder technology production method to increase all the properties of the green compact and non-compact parts by thermal process to bond the green particles to obtain the desired properties. It should be noted that many parameters control the sintering process including the dependent and independent variables. A rational theory of sintering should predict the routes of production of the required structure of sintered body in order to provide its physico-chemical and physico-mechanical properties which are determined by this structure [2].

Modeling is one of the most crucial element in the design and optimization of thermal materials processing systems. Practical processes and systems are generally very complicated and must be simplified through idealizations and approximations to make the problem solvable. This process of simplifying a given problem so that it may be represented in terms of a system of equations, for analysis, or a physical arrangement, for experimentation, is termed modeling. Once a model is obtained, it is subjected to a variety of operating conditions and design variations. If the model is a good representation of the actual system under consideration, the outputs obtained from the model characterize the behavior of the given system. This information is used in the design process as well as in obtaining and comparing alternative designs by predicting the performance of each design, ultimately leading to an optimal design [3].

Many studies have been made to determine the mechanisms involved during sintering process. Few researches have studied the influence of particle size, shrinkage, porosity, grain growth, densification and micro-structural evolution during conventional sintering. Besides, all these they have studied time and temperature distribution during this process. More models that are sophisticated and taking superposition's of various sintering mechanisms into account such as references [4 and 5].

Therefore, the present research is an attempt to understand the sintering phenomenon through developing a mathematical model. An axisymetric finite-difference time domain model has been developed to simulate the complete

temperature response of the system. The general heat equation was discretized , as well as the boundary conditions.

2. Mathematical Model

Several attempts have been made to study some parameters in sintered sample by different techniques. One of these parameters is temperature distribution. Due to its time depending, the techniques are usually employed in time domain. Heat transfer model has been conducted to characterize the temperature distribution in the specimen and its evaluation during field activated sintering. Significant temperature gradients were found in specimen in both radial and axial directions.

The transient heat transfer is described by the well-known energy balance equation [6].

Energy in left face + heat generated with element = change in internal energy + energy conducted out right face +heat convection

Combining the relations above gives:

$$-kA\frac{\partial T}{\partial X}+q^{\circ}A\,dX=\rho c\,A\frac{\partial T}{\partial t}\,dX-A\left[k\frac{\partial T}{\partial X}+\frac{\partial}{\partial X}\left(k\frac{\partial T}{\partial X}\right)dX\right]+hA\left(T-T_{\infty}\right) \quad \ldots\ldots(1)$$

This relationship applies to system of any size, shape or material. For the present work, the materials treated are assumed to be cylindrical. The dimensions of the specimen which was used in assumption are: H = 60mm and D = 30mm. Figure 1 represents the cylindrical coordinates of the specimen.

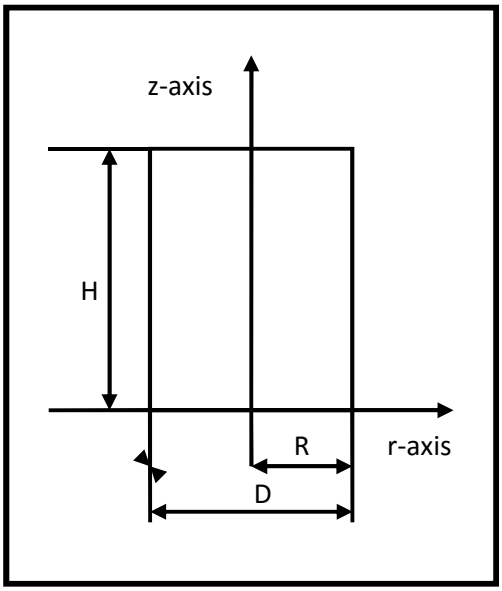

Figure: 1 The cylindrical coordinate system.

A 3- dimentional heat conduction equation at the point whose cylindrical coordinates are (r , z) is

$$\frac{1}{\alpha}\frac{\partial T}{\partial t}=\frac{\partial^2 T}{\partial r^2}+\frac{1}{r}\frac{\partial T}{\partial r}+\frac{1}{r^2}\frac{\partial^2 T}{\partial \phi^2}+\frac{\partial^2 T}{\partial z^2}+\frac{q^{o}}{k} \qquad \ldots\ldots\ldots(2)$$

where $\alpha = \frac{k}{\rho c}$

Adams and Rogers [7] showed that when the cylinder is solid rather than hollow special consideration must be given to the central node at r = 0. At r = 0, the second term in equation 2, $\left(\frac{1}{r}\right)\left(\frac{\partial T}{\partial r}\right)$ is indeterminate and equal to $\frac{\partial^2 T}{\partial r^2}$,this term evaluated by using L'Hopital's rule.

If one uses these results, the governing partial differential equation at r = 0 can be written:

$$\frac{1}{\alpha}\frac{\partial T}{\partial t} = \frac{\partial^2 T}{\partial r^2} + \frac{\partial^2 T}{\partial r^2} + \frac{\partial^2 T}{\partial z^2} + \frac{q^\circ}{k} \qquad \text{...……...(3)}$$

Another two-dimensional of practical importance is two-dimensional transient conduction in the radial and depth directions. For this model T = T (r, z, t) and equation 2 reduces to:

$$\frac{1}{\alpha}\frac{\partial T}{\partial t} = \frac{\partial^2 T}{\partial r^2} + \frac{1}{r}\frac{\partial T}{\partial r} + \frac{\partial^2 T}{\partial z^2} + \frac{q^\circ}{k} \qquad \text{...……...(4)}$$

The following initial and boundary conditions are presented as shown in figure 2.

i) Initial conditions:

T (r, z, 0) = T_o

T (r, 0, 0) = T_o

T (0, z, 0) = T_o

When z=0, $\frac{\partial T}{\partial z} = 0$

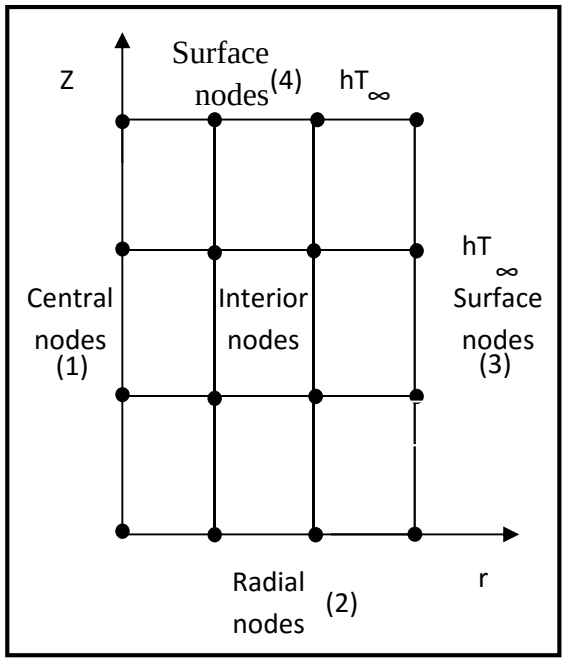

Figure: 2 Boundary conditions of material is assumed to be cylindrical.

ii) Boundary conditions:

The interior nodes, surface (1) and surface (2), the heat effected is conduction only, then the heat equations represented on these sides are illustrated in equation (٣).

The heat transfer effected on surface (3) and surface (4) are conduction and convection then the boundary conditions on these sides are:

$$-\ k\ A\ \frac{\partial T}{\partial r} = h\ A\ (T - T_{\infty}) \qquad \text{..... (٥)}$$

Then the equation of the governing heat transfer is represented as

$$\frac{1}{\alpha}\frac{\partial T}{\partial t} + \frac{h\,p}{Ak}\,(T - T_{\infty}) = \frac{\partial^2 T}{\partial r^2} + \frac{1}{r}\frac{\partial T}{\partial r} + \frac{\partial^2 T}{\partial z^2} + \frac{q^{\circ}}{k} \qquad \text{.....(٦)}$$

It is necessary to use the finite difference approximation to the partial differential equation (PDEs), so that the problem could be solved by a computer. It has been considered the approximation is in the region over which we have laid an orthogonal grid with an equal spacing (the distance between neighbouring points). The indices i and j will be used for indicating the points along the r and z directions and the index n will be used for indicating the points over the time layers. We shall use the approximation of the first order of accuracy for time, and the second order of accuracy for space. The distance between the points in the established grid are Δr, Δz and Δt. the grid is represented in Figure 3. Notice that the temperature values in the time layer n are known and we search for temperature values of the time n+1, the partial derivative with respect to time is approximated by forward-difference scheme:

The finite difference form of the governing equation ٣ can be written as:

$$\frac{2}{(\Delta r)^2}\left(T^{\,n}_{i+1,\,j} - 2\,T^{\,n}_{i,\,j} + T^{\,n}_{i-1,\,j}\right) + \frac{1}{(\Delta z)^2}$$

$$\left(T^{\,n}_{i,\,j+1} - 2\,T^{\,n}_{i,\,j} + T^{\,n}_{i,\,j-1}\right) + \frac{q^{\circ}}{k} = \frac{1}{\alpha}\left(\frac{T^{\,n+1}_{i,\,j} - T^{\,n}_{i,\,j}}{\Delta t}\right) \qquad \text{.....(٧)}$$

And for equation ٤ as:

$$\frac{1}{(\Delta r)^2}\left(T^{\,n}_{i+1,\,j} - 2\,T^{\,n}_{i,\,j} + T^{\,n}_{i-1,\,j}\right) + \frac{1}{r\,(i)}\,\frac{\left(T^{\,n}_{i+1,\,j} - T^{\,n}_{i-1,\,j}\right)}{2\,\Delta r} +$$

$$\frac{1}{(\Delta z)^2}\left(T^{\,n}_{i,\,j+1} - 2\,T^{\,n}_{i,\,j} + T^{\,n}_{i,\,j-1}\right) + \frac{q^{\circ}}{k} = \frac{1}{\alpha}\left(\frac{T^{\,n+1}_{i,\,j} - T^{\,n}_{i,\,j}}{\Delta t}\right) \qquad \text{.....(٨)}$$

And for equation 11

$$\frac{1}{(\Delta r)^2}\left(T^{\,n}_{i+1,\,j} - 2\,T^{\,n}_{i,\,j} + T^{\,n}_{i-1,\,j}\right) + \frac{1}{r\,(i)}\,\frac{\left(T^{\,n}_{i+1,\,j} - T^{\,n}_{i-1,\,j}\right)}{2\,\Delta r} + \frac{1}{(\Delta z)^2}$$

$$\left(T^{\,n}_{i,\,j+1} - 2\,T^{\,n}_{i,\,j} + T^{\,n}_{i,\,j-1}\right) + \frac{q^{\circ}}{k} = \frac{1}{\alpha}\left(\frac{T^{\,n+1}_{i,\,j} - T^{\,n}_{i,\,j}}{\Delta t}\right) + \frac{h\,p}{Ak}\left(T_i^{\,n} - T_{\infty}^{\,n}\right) \qquad \text{.....(9)}$$

Equations 7, 8 and 9 are so called explicit formulation of equations 3, 4 and 6 In the explicit formulation, there is only one point at the n+1 layer, and the temperature at that point, which can be easily calculated from the values of the previous time layer.

Finite difference method is devoted to basic techniques for solving parabolic PDEs. Typical explicit approximation has been explained. The computer program

gives more reliability to calculate temperature profile against r and z coordinates depending upon the boundary conditions. That gives different form of equation 5 in explicit finite difference technique. principles of stability analysis with numerical schemes are discussed by *Anderson et al.* [6], where $\lambda = \frac{\alpha \Delta t}{(\Delta r)^2}$ is the convergence factor, and assuming that Δr = Δz. More details for numerical solution which was given by *Elham* [8].

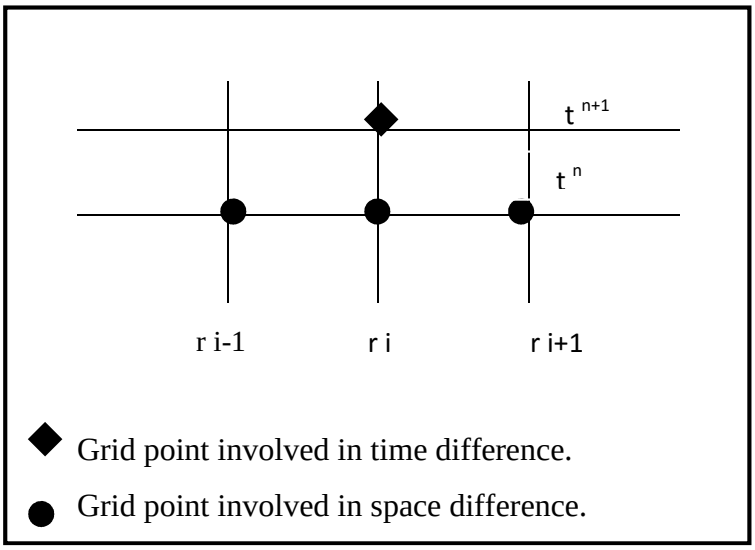

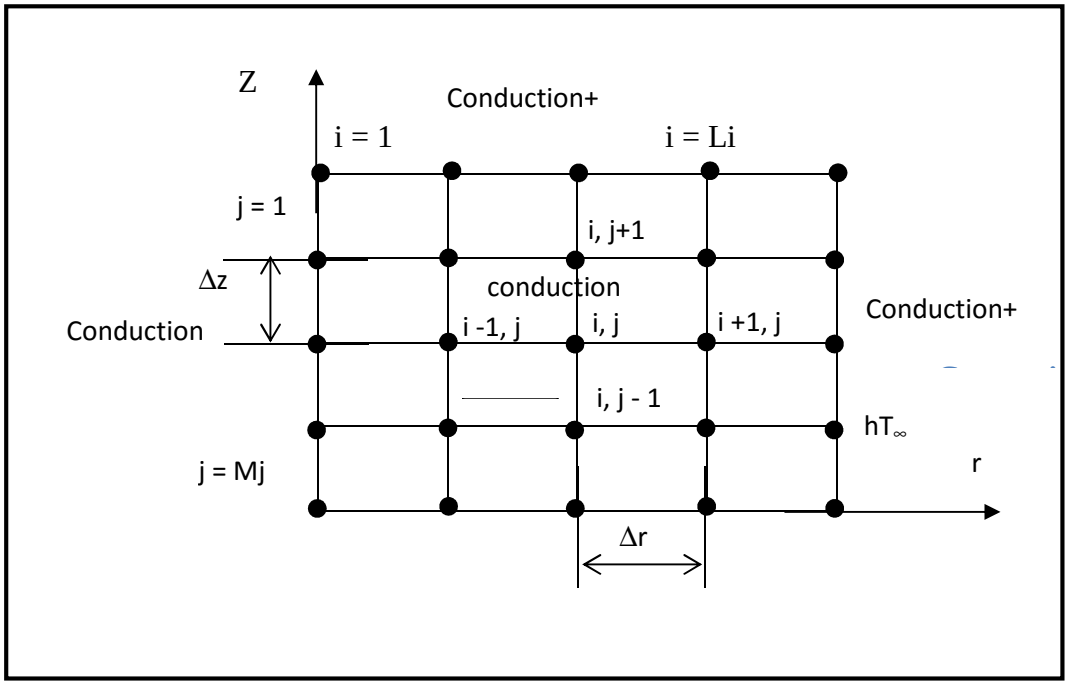

Figure 3 Computational grid of the cylindrical model.

3. Calculating of Various Parameters:

The Simulation is intended for use as atool to explore the effects of the various parameters on temperature distribution, such as grain growth, density, porosity and relative strength.

3.1. Calculating of Grain Growth

Several computer simulation models for normal grain growth have been developed.The following equation is used to simulate the grain growth behavior during sintering [9].

$$\frac{d\,G}{d\,t} = \frac{a\ \exp\ \left(-Q_a / R\,T\right)}{G} \qquad \text{……. (10)}$$

Where a is a absorption coefficient = 0.007 m^2/s
By using explicit formulation, the equation (10) becomes:

$$G_{i,j}^{\,n+1} = \left[\left(\frac{a \exp\ \left(-Q_a / RT_{i,j}\right)}{G}\right) * \Delta t\right] + G_{i,j}^{\,n} \qquad \text{..……(11)}$$

3.2. Calculating OF Density

The densification rate equation in the final stage of sintering is described as [10] :

$$\frac{d\rho}{dt} = \frac{288\ \ D_L\,\gamma_s V_m}{R\ T\ G^{\,n}} \qquad \text{…… (12)}$$

Where D_L is the lattice diffusion coefficient = 13.6 m^2/s, γ_s is the specific surface energy = 0.71 J/m^2 , V_m is molar volume =12.84*10^{-6} m^3/mol, and n is a constant = 3 for lattice diffusion. These value where given in Ref.[10].

It can be written by using explicit formulation, so equation (12) becomes:

$$\rho_{i,j}^{\,n+1} = \left[\left(\frac{288\ \ D_L\,\gamma_s V_m}{R\,G^{\,3}} * \frac{1}{T_{i,j}}\right) * \Delta t\right] + \rho_{i,j}^{\,n} \qquad \text{...…..……(13)}$$

In order to calculate the density distribution through sintering time, it should be depended upon the value of theoretical density.

3.3. Calculating of Porosity

The porosity can be calculated due to the references [11] as:

$$\theta = 1 - \frac{\rho}{\rho_{th}} \qquad \text{……. (14)}$$

3.4. Calculating of Relative Strength

Tensile strength (σ_c) is a function of porosity (θ), so the relative strength (σ_c / σ_{co}) depends on porosity (θ). The relation between relative strength and porosity is given by Ref.[11].

$$\sigma_c / \sigma_{co}\ \left(1 - 1.21\ \theta^{\,2/3}\right) \qquad \text{……..(15)}$$

The flowchart used to show the basic procedure of the solution approach is given in figure 4.

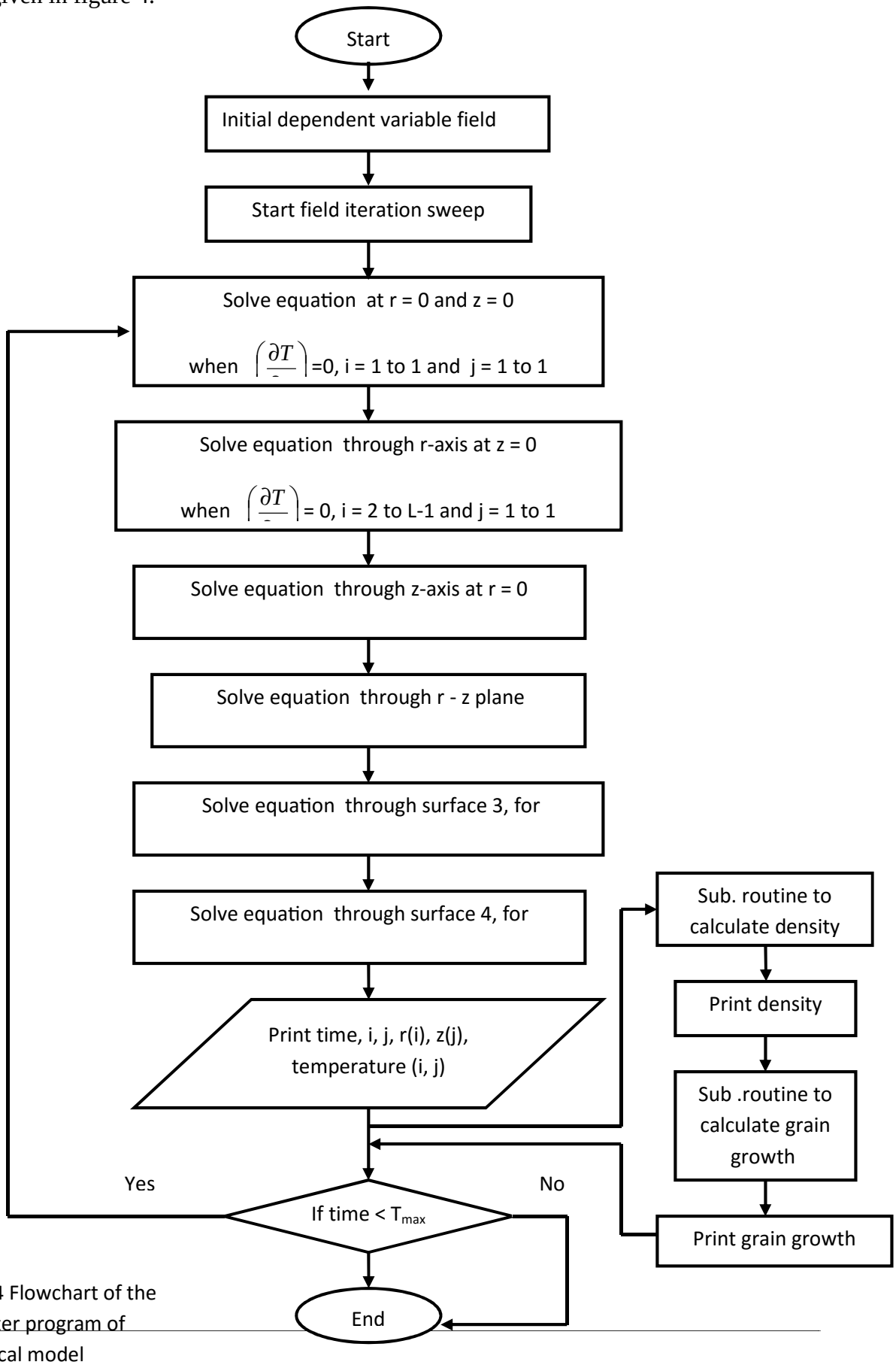

Figure 4 Flowchart of the computer program of cylindrical model

4. Results and Discussion

In order to develop simple sintering equations for the various mechanisms, it is necessary to idealize the structure of the powder system to allow it to be analyzed mathematically. In the analytical models, the particles are assumed to be spherical and of the same size. Furthermore, the consolidated powder form is assumed to have a uniform packing arrangement.

Alumina powder compacts are sintered at fixed temperature 1610 ^{o}C, with a time 8100 second. The effect of green compact and particle size is considered. Alumina compact of green density equals 2610 Kg /m^3 [13].

4.1. Effect of Temperature

Figure 5 shows the relationship between time and temperature during the sintering cycle for alumina. The temperature in alumina compact increases with the time and reaches a certain temperature of sintering after 8100 second.

Figure 6 shows a series of sintering temperature data at radial direction of cylindrical samples during isothermal sintering alumina. It has been shown that the temperature distribution in the different times and depths. This was shows the different spatial and temporal temperature distribution of interior nodes of sample.

Figure 7 shows the Isothermal temperature contour map for sintering alumina samples, It shows the distribution of maximum sintering temperature on the r-z plane.

Figure 8 describe surface temperature distribution mesh for sintering alumina. This figures explain the gradient of temperature in the samples when they are heated from room temperature to sintering temperature.

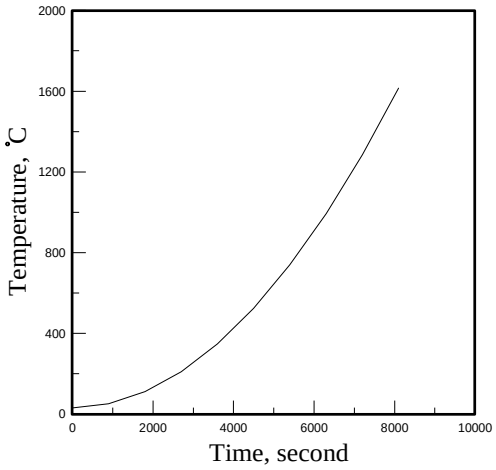

Figure 5 Temporal variation in temperature in alumina.

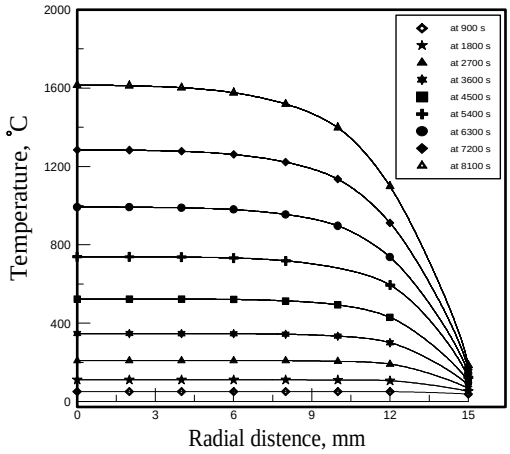

Figure 6 Interior temperature profile against radial d for alumina in different depths and times.

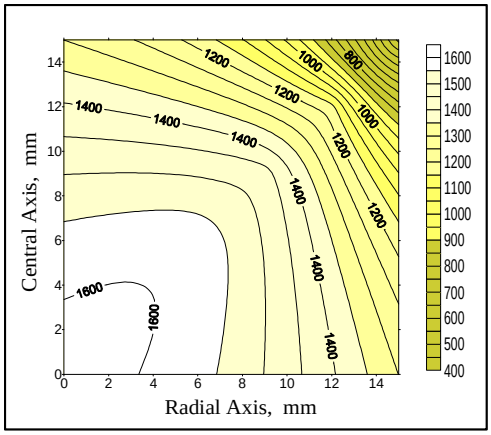

Figure 7 Isothermal contour map for sintering for sintering alumina at 8100 second.

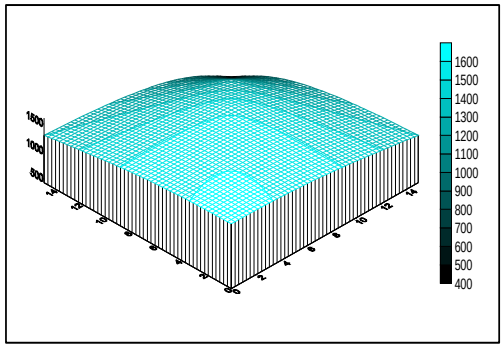

Figure 8 Surface temperature distribution mesh alumina at 8100 second.

4.2. Effect of Grain Size

Figure 9 shows that the grain size increases with the sintering time for alumina after 8100 second, it shows that the grain size reach to value 2.1 μm at the center point of specimen 0, 0.

Figure 10 shows that the grain size increases with the sintering time for alumina after 8100 second, it shows that the grain size reach to value 2.1 μm at the center point of specimen

Figure 11 shows the contour map of grain size distribution with the radial and axial distances for alumina. It has been shown that the grain growth is a function of temperature and decreased forward the wall and the surface.

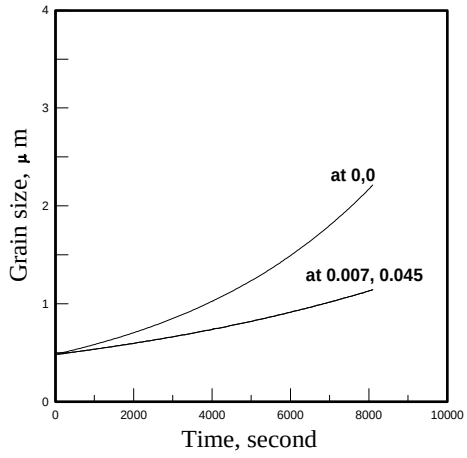

Figure 9 Variation in grain size of alumina alumina for different times.

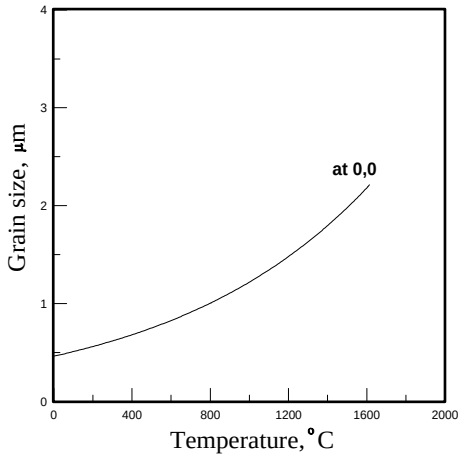

Figure 10 Variation in grain size of with sintering temperature at center point.

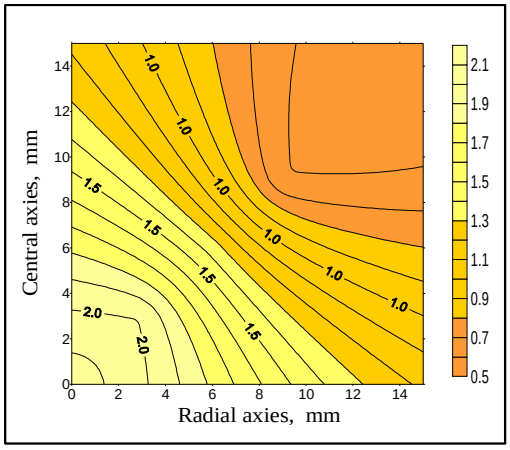

Figure 11 Contour map of grain size for sintering alumina at 8100 second.

4.3. Effect of Density

Figure 12 shows the relation between the density and time for alumina. Full density for example at center point 0, 0 reaches 94.8% TD after 8100 seconds by conventional sintering.

The relation between the density and temperature is clear in figures 13 at point 0, 0 for alumina. It has been shown that the density of alumina increases as the sintering temperature increase and reach to 3.7 g/cm^3 at temperature 1610 ^{o}C.

Figure 14 shows the three dimension contour map for density distribution of alumina from the bottom to the surface of the sample. It has been shown that the density is a function of temperature and decreases forward the wall and the surface.

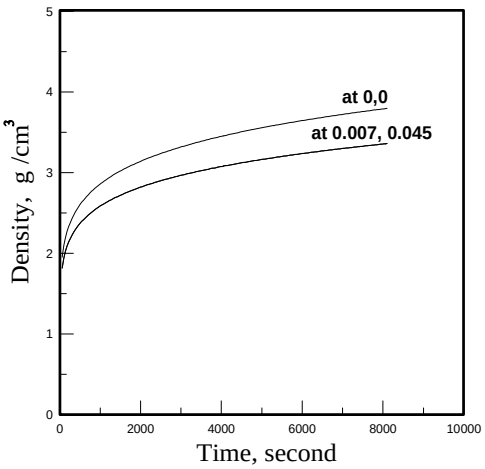

Figure 12 Variation in density of alumina alumina with sintering time.

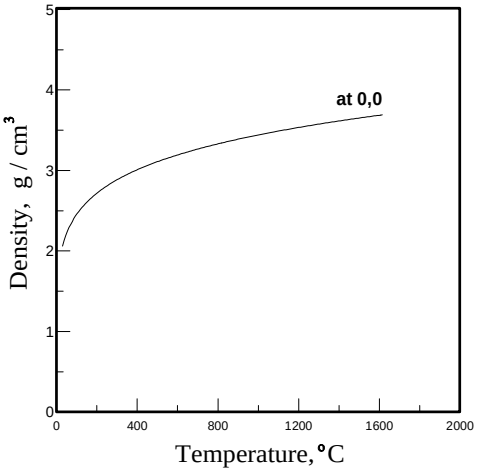

Figure 13 Variation in density of with sintering temperature at center point.

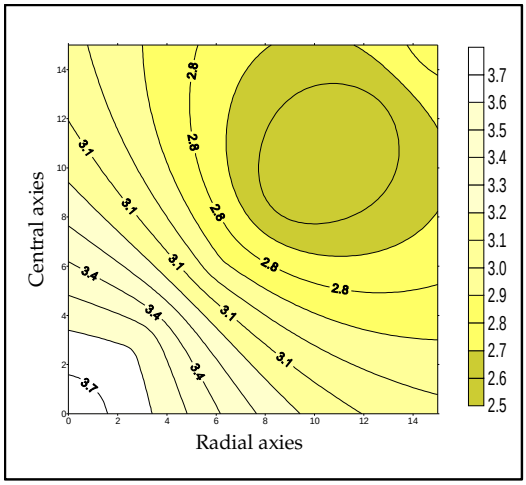

Figure 14 Contour map of density distribution for sintering alumina at 8100 second.

4.4. Effect of Porosity

Figure 15 shows initially the porosity for alumina compact was 43%, during sintering after 8100 second the open porosity decreases continuously to reach 0.5% at center point 0, 0.

Figures 16 show the variation of porosity in alumina with the temperature, the porosity high decreases when the temperature increases. At center point 0, 0 the porosity of alumina decreases from 43% to 0.5% at temperature 1610 ^{o}C,

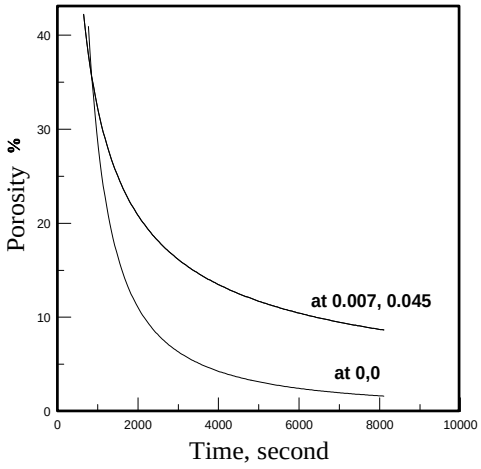

Figure 15 Porosity evolution during sintering alumina versus time.

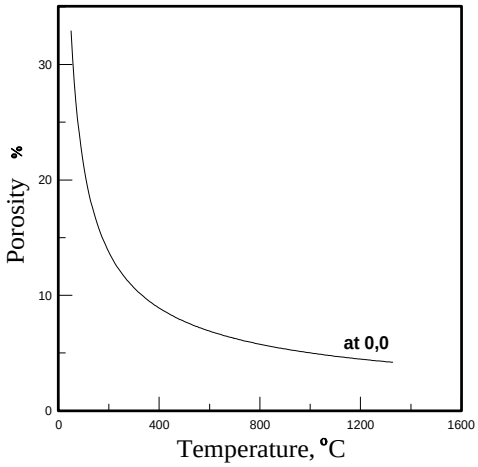

Figure 16 Porosity evolution during sintering alumina versus temperature at center point.

4.5. Effect of Relative Strength

Figure 17 shows the variation in relative strength with the time in alumina, it has been shown that it increases from 0.309 to 0.964 at center point 0, 0 after 8100 second.

Figures 18 shows the relation between relative strength and temperature in alumina sample at center point 0, 0. It has been shown that the relative strength

increases with temperature. For alumina the relative strength increases from initial 0.309 to 0.964 at temperature 1610 ^{o}C.

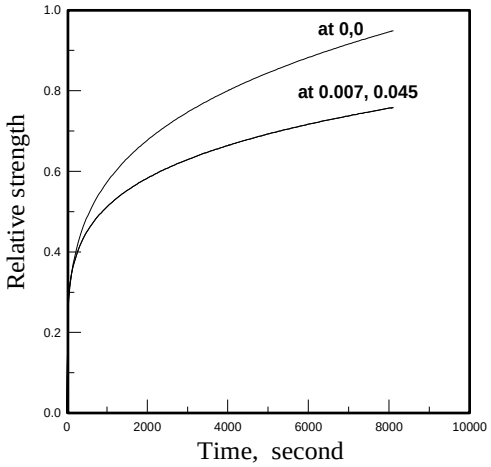

Figure 17 Relative strength of alumina as

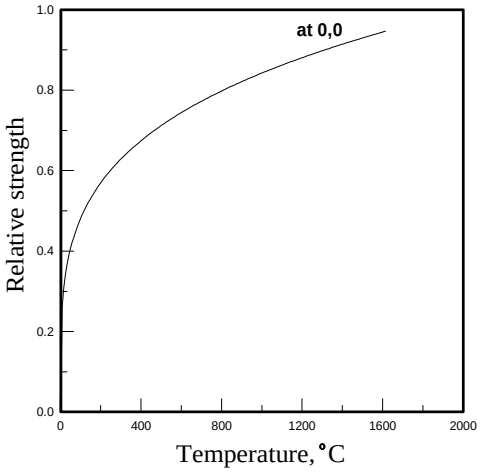

Figure 18 Relative strength of alumina as a function

5. Conclusions

In the present work is done to understand the sintering mechanisms through mathematical model. An axisymmetric finite-difference model with the explicit technique is developed to simulate the complete temperature response of the system.

By using mathematical model for temperature distribution one can be predict the temperature at all point of the sample during sintering.. The temperature is the main factor to predict what happens during sintering and it will be as a function of other properties. The grain size for alumina increases as temperature increases without reaching the coarsening stage. The density increases as the temperature increases, it reaches to about 94.8% TD at center point.

As the temperature increases, other properties such as porosity and relative strength vary. The porosity is a function of density and relative strength, so the porosity decreases with increase in the density. The relative strength is calculated as a function of porosity. It is increases when the porosity decreases.

It should be shown that the model gives a good reliability and validation with experimental and theoretical work available.

Nomenclature

Symbol	Mean	Unit
A	**Area of sample**	**m^2**
c	**Specific heat**	**J/kg .^{o}C**
D_L	**Lattice diffusion coefficient**	**m^2/s**

Symbol	Mean	Unit
G	The mean grain size	m
$G^{n}_{I,j}$	Initial grain growth	m
$G^{n+1}_{i,j}$	New grain growth	m
h	Heat transfer coefficient	$W/m^2.{}^oC$
k	Thermal conductivity	$W/m.{}^oC$
Q_a	Activation energy for grain growth	kJ/mol
$q°$	Heat generated with element	W/m^3
R	Gas constant	J/mol. K
r	Radius of the sample	m
Δr	Change in radial	m
T	Temperature of the sample	^oC
T_∞	Ambient temperature	^oC
T_s	Sintering temperature	^oC
Δt	Chang in time	sec
V_m	Molar volume	m^3/mol
λ	Convergence factor	
α	Thermal diffusivity	m^2/s
ρ	density	kg/m^3
ρ_{th}	Theoretical density	kg/m^3
$\rho^{n}_{I,j}$	Initial relative density	
$\rho^{n+1}_{i,j}$	New relative density	
γ_s	Specific surface energy	J/m^2
θ	Porosity	%
σ_C	Tensile strength	kg/m^2
σ_{Co}	Tensile strength of fully dense material	kg/m^2
σ_C/σ_{Co}	Relative strength	

6. References

1. H. Riedel and T. Kraft, "Simulation in Powder Technology," Continuum Scale Simulation of Engineering Materials, Fundamental Microstructures–Process Applications, Wiley-VCH Verlag GmbH & Co. KgaA , 5 (2004) 473.

2. E. Olevskya, and A. Molinari, "Instability of Sintering of Porous Bodies," International journal of plasticity, 16 (2000) 1.

3. Y. Jaluria, "Thermal Processing of Materials: From Basic Research to Engineering," ASM, J. of Heat Transfer, 125 (2003) 957.

4. T. Kraft, and H. Riedel, "Numerical Simulation of Solid State Sintring; Model and Application", Journal of the European Ceramic Society, 24 (2004) 345.

5. W. Fahrenholtz, "Ceramic Engineering III Sintering," Technical Report by Ceramic Engineering Department, University of MissouriRolla, 2004, www.ranews.info/articles/jf02top.htm.

6. G. Holman, "Heat Transfer," 4th Edition, Mc Graw-Hill Kogakusha, Ltd, 1976, pp. 2-6.

7. A. Adams, and D. Rogers, "computer-Aided Heat Transfer Analysis," Mc Graw-Hill, 1973.

8. D. Anderson, , J. Tennchill, and R. pletcher, "Computational Fluid Mechanics and Heat Transfer," Mc Graw-Hill, 1984.

9. E . Ibraheem, " Predictive Study for Optimum Sintering Parameters for Oxide Ceramics," Ph.D.,Thesis, University of Technology, Iraq, 2006

10. R. Zhang, and R. Engel, "Sintering Simulation of Stainless Steel Powder Compacts," J. XXI ICTAM, Warsaw, Poland, 15 (2004).

11. S. Kang, and Y. Jung, "A Model for the Densification at Final Stage Sintering: Lattice and Grain Boundary Diffusion," Department of Material Science and Engineering, Republic of Korea, 2004, www.mri.psu.edu/conferences/sint03.

12. E. Olevskya, and A. Molinari, "Instability of Sintering of Porous Bodies," International journal of plasticity, 16 (2000) 1.

13. E. Olevskyi, R. German and A. Upadhyaya, "Effect of Gravity on Dimensional Change During Sintering II. Shap Distortion," J.Acta Metalyrgica, 48 (2000)

14. B. Latella and T. Liu, "High-Temperature Young's Modulus of Alumina During Sintering," J. Am. Ceram. Soc., 3 (2005) 773.